

A SYSTEMATIC APPROACH TO MODEL AND OPTIMIZE QUALITIES OF CASTINGS PRODUCED BY SQUEEZE CASTING PROCESS

Dashuang Zhou, Xiaoping Su , Chuang Yang and Zhengyang Kang

School of Mechanical and Power Engineering, Nanjing Tech University, Nanjing, Jiangsu 211816, China

Zhi Li

School of Automotive and Traffic Engineering, HuBei University of Arts and Science, Xiangyang City 441053, China

Copyright © 2022 American Foundry Society
<https://doi.org/10.1007/s40962-022-00887-6>

Abstract

The present study attempts to promote the quality of squeeze casting components by a two-stage study which includes experimental research of virtual casting based on response surface method (RSM) and experimental research of actual production casting. In the first stage, the critical parameters determined by the numerical model of casting procedure indicate that the qualities of castings, including casting solidification time, secondary dendrite spacing and porosity, are highly affected by the die temperature, pouring temperature and filling velocity. The input–output relationship developed, based on Box–Behnken experimental design (BBD), is found to be statistically adequate and yielded better prediction accuracy. NSGA-II algorithm

performs multi-directional search in multi-dimensional space simultaneously combining with the data optimization software ISIGHT. In the second stage, the trial production test was carried out on the squeeze casting machine to verify the optimal parameters. X-ray inspection, metallographic structure testing and mechanics performance testing show that the casting has no casting defects and has good mechanical properties.

Keywords: Squeeze casting, virtual casting, response surface methodology, optimization

Introduction

Squeeze casting process is a prominent casting method to achieve good mechanical properties combined with less porosity, less oxide inclusions and fine microstructure.¹ The squeeze casting process is also widely applied in automobile industries as a near-net forming technology without too much subsequent processing.^{2,3} In particular, for the global energy crisis and the increasing demand for lightweight products, squeeze casting is an effective way to achieve energy saving and also conducive to the development of new energy vehicles.

Recently, squeeze casting has been studied widely. For example, the effects of processing variables on the fluidity of Al–Si alloy melt during squeeze casting and high-pressure rheo-squeeze casting on Fe-containing intermetallic

compounds and mechanical properties of Al–17Si–2Fe–(0, 0.8) V alloys are investigated.^{4,5} Also, squeeze casting was used to fabricate composites, which are lightweight structural materials with potential applications in the automotive industry.⁶ In addition, the macrostructure such as Si phase morphology, dislocation density, mechanical properties and friction and wear properties of Al–Si–Cu–Mg alloys were studied under squeeze casting process.⁷ However, these works are limited to the study of squeeze casting process, and the relationship between casting process parameters and casting quality is not considered. The selected process parameters are essential for obtaining a sound casting.⁸ Meanwhile, for conventional engineering research approach, the effects of variables are studied by changing one parameter at a time.

Recently, some intelligent optimization algorithms or experimental methods have been introduced to analyze squeeze casting process. M. Arulraj et al. focused on parametric optimization of squeeze cast hybrid (LM24–

SiC_p-coconut shell ash) composite through Taguchi method and genetic algorithm.⁹ Sarfraz et al. investigated the effects of process parameters on mechanical and microstructural characteristics of Al 6061-SiC composite fabricated via squeeze casting and used Box-Behnken experimental design to arrange the test.¹⁰ M Thirumal Azhagan et al. developed the different grades of aluminum alloy composites by squeeze casting process and used Taguchi method to conduct the parametric optimization.¹¹ Hassasi et al. investigated the effects of squeeze casting parameters on the mechanical properties, microstructure characteristics and wear behavior of A390 aluminum alloy based on the Taguchi method.^{12,13}

The real-time observation of casting process is still challenging, especially for the multi-factors analyzing and quantitatively evaluating casting quality. Hence, various numerical simulation and calculation tools have been employed to predict the casting defects for the known set of process variables, without conducting the actual experiments. Krishna et al. performed numerical simulations in MAGMASOFT and combined the analysis results with actual measurements to effectively estimated IHTC.¹⁴ Li et al. took the automobile control arm as the research object, using MAGMASOFT to simulate the squeeze casting process, and predicted the position of the shrinkage cavity and shrinkage defects in the casting process accurately.¹⁵ Hu et al. introduced a novel method for predicting the particulate flow and distribution of particulate reinforced metal matrix composites in mold filling based on numerical simulation.¹⁶ Sanil et al. used squeeze casting process to replace the gravity casting method to attain better performance of the pistons and studied the composition by numerical steady-state thermal analysis using ANSYS Workbench to obtain a maximum heat flux.¹⁷ Li et al. solved the casting defects of the gearbox cover. And the ProCAST was taken to simulate the squeeze casting process and predict the position of shrinkage defects accurately.¹⁸ Borlepwar, et al. utilized DOE and flow simulation to analyze shrinkage defects in high-pressure casting process.²⁰ Pan Fan, et al. implemented the model of the wheel casting process within FLUENT, a commercial Computational Fluid Dynamics (CFD) software package. Examination and simulation of silicon macrosegregation in A356 wheel casting were studied, and porosity in A356 wheel casting was predicted.^{19,21} In addition, Sui et al. convinced that the development and application of numerical simulation technology in the foundry is playing an important role for designing and optimizing the casting parameters and verified that their simulation and experimental results are almost consistent.^{22,23} G. Ruff, T.E. Prucha, et al. also mentioned that a critical feature for the proper implementation and use of casting is the application of computer-aided process simulation and modeling.²⁴

Based on above, more research efforts are needed for developing model, simulating and optimizing the squeeze

process defects with intelligent manufacturing technology. There is a significant scope to systematically study to model, simulate and optimize the squeeze process using statistical and soft computing tools. Hence, this paper aims to propose a two-stage casting approach, virtual casting based on RSM and actual production casting, to model and optimize qualities of squeeze casting.

Modeling and Optimization Details

The steps followed to model and optimize are illustrated in Figure 1.

The steps below introduce the details of the present study, including modeling and optimization of castings in squeeze casting process. Figure 2 shows the casting model.

Step 1 Selection of variables and levels

Higher squeeze pressure will have demand on high-tonnage equipment facility and more capital investment. On the other hand, low squeeze pressure might not be sufficient to eliminate the accumulated gases between die-metal interfaces, resulting in poor interfacial heat transfer.

In squeeze casting, the setting of pouring temperature should consider the squeeze casting method, casting structure, alloy composition and other factors comprehensively.²⁵ And it will have an important impact on the casting forming quality and the service life of the die. If the pouring temperature is too low, it is easy to appear the phenomenon of the front-end metal liquid solidification in advance in the mold filling process, which not only increases the flow resistance of the metal liquid, making the mold filling difficult, but also greatly reduces the pressure effect of the punch, unable to achieve the purpose of casting solidification under high pressure. If the pouring temperature is too high, can obtain better liquidity, but at the same time, the performance of metal suction is stronger, cooling gradient grows wider, the cooling crystallization in the volume shrinkage of quantitative change is big, easy to form defects such as shrinkage and hot crack. In addition, higher pouring temperature can produce larger thermal erosion to the mold, affecting the service life. For indirect squeeze casting, because of high specific pressure, so the pouring temperature will be appropriately lowered, which can reduce the suction effect of the metal liquid and reduce its solidification process.²⁶ The volume shrinkage can also reduce the thermal erosion of metal liquid on the mold.

The die temperature has also an important effect on casting quality.²⁷ Too low temperatures for die will result in inadequate fluidity, cold laps on the casting surface and thermal fatigue failures in the die, whereas higher temperature cause extrusion of liquid metal at die interfaces,

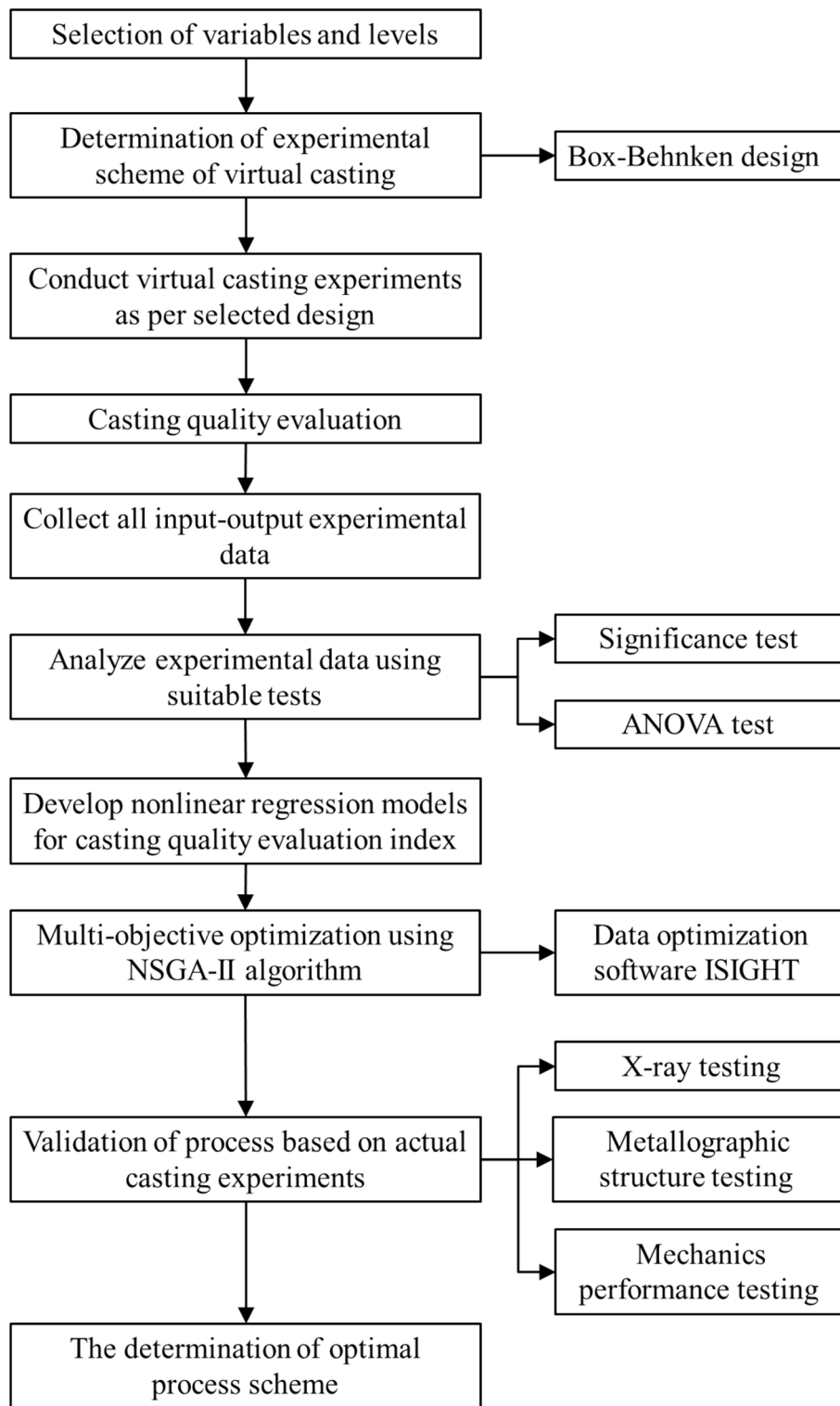


Figure 1. Methodology applied for modeling and optimization.

shrinkage and hot spots in the castings. On the other hand, high temperature might increase the solidification time. On the contrary, low temperature for die will result in premature solidification.

Filling velocity refers to the advance velocity of the punch, the metal liquid filling cavity under the pressure of the punch. It will directly affect the flow state of liquid metal. If the filling velocity is too slow, part of the metal liquid is prone to advance in the filling process solidification phenomenon, the formation of metal shell leads to extrusion

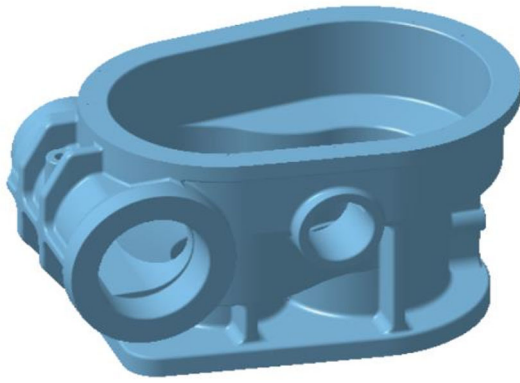


Figure 2. CAD model of aluminum alloy gearbox case.

pressure transmission blocked, resulting in poor compression effect. If the filling velocity is too fast, the gas in the cavity is difficult to discharge in time, and it is easy to discharge at the thickness change of the casting, at the corner and at the confluence of metal liquid turbulent flow leads to defects such as porosity and shrinkage after casting forming. For indirect squeeze casting, the punch usually pushes liquid metal through the inner gate into the mold at a lower speed at the front of the mold filling cavity, prevents metal liquid from producing gas and ensures smooth filling. At the end of filling, filling speed is usually accelerated to avoid gold the effect of pressure is weakened by the early solidification of the liquid.

The choice of input variables and decision on the operating levels are of paramount importance to establish control over the process and minimize the defects. Too wide operating range of variables may result in an infeasible solution on the response surface. Conversely, too narrow range will result in incomplete or poor information about the process.

Therefore, consulting available literature, expert's advice from foundry personal and trial experiments conducted in the research laboratory are used to select process variables and set their operating range.

Step 2 Virtual casting

After determining the experimental variables and levels, Box–Behnken design (BBD) method based on spherical space design is adopted to arrange the experiments. This method tries to reflect the influence rule of each experimental factor on the casting quality with the least number of tests. Considering the difference of grid division may lead to the error of calculation results, Therefore, a total of 29 trial plans are arranged, including 5 central repeated trials. The specific experimental arrangements are presented in Table 1.

Step 3 Casting quality evaluation

Table 1. BBD Experimental Schemes

Exp. no.	Experimental factor			
	T_p [°C]	V_f [m/s]	V_s [m/s]	T_c [°C]
1	L-2	L-2	L-2	L-3
2	L-2	L-1	L-2	L-2
3	L-3	L-2	L-2	L-2
4	L-1	L-2	L-2	L-2
5	L-2	L-2	L-2	L-2
6	L-2	L-2	L-3	L-3
7	L-1	L-2	L-3	L-2
8	L-2	L-2	L-3	L-1
9	L-2	L-3	L-1	L-2
10	L-1	L-2	L-2	L-3
11	L-3	L-2	L-2	L-3
12	L-2	L-2	L-1	L-3
13	L-2	L-2	L-2	L-2
14	L-1	L-3	L-2	L-2
15	L-2	L-1	L-3	L-2
16	L-2	L-1	L-2	L-3
17	L-2	L-3	L-2	L-1
18	L-3	L-1	L-2	L-2
19	L-2	L-1	L-1	L-2
20	L-3	L-2	L-2	L-1
21	L-2	L-2	L-2	L-2
22	L-2	L-1	L-2	L-1
23	L-1	L-2	L-1	L-2
24	L-2	L-3	L-3	L-2
25	L-3	L-2	L-1	L-2
26	L-2	L-2	L-1	L-1
27	L-2	L-2	L-2	L-2
28	L-1	L-2	L-2	L-1
29	L-3	L-2	L-3	L-2

The evaluation index of casting defect is the key to the analysis of virtual casting experiments results. Porosity defect is a common defect in squeeze casting, which will directly affect the mechanical properties and fatigue life of the casting. In addition, the secondary dendrite arm spacing (SDAS) has an important effect on the mechanical properties of castings. Therefore, it is helpful to predict the formation of porosity and dendrite spacing during casting solidification to control casting quality. In addition, the solidification time of casting is related to the production efficiency. On the premise of guaranteeing the forming quality of the casting, make the solidification time shorter, the process cycle will be the shorter.

Table 2. Chemical Composition of Casting and Die Material

Elements	Si	Mg	Fe	Mn	Zn	Cu	Ti	Al
Casting/ Weight(%)	6.5-7.5	0.25-0.45	0.05-0.2	0.01-0.1	0.01-0.1	0.1-0.2	0.1-0.2	Balance
Elements	C	Cr	Si	Mo	Mn	Ni	N	Fe
Die/ Weight(%)	0.019	25.387	0.328	3.77	0.738	6.714	0.028	Balance

Step 4 Develop nonlinear regression models between process parameters of squeeze casting and casting defect evaluation indexes, statistical analysis and performance evaluation

The experimental data as per the design matrices shown in Table 2 are utilized to develop nonlinear regression models for the evaluation index of casting quality, namely porosity, SDAS and solidification time. The coefficients are determined initially by collecting input–output data of the process and later performing model building through regression analysis. The collected experimental input–output data are analyzed and nonlinear input–output relations are developed. The models developed have been tested for their statistical adequacy and significance with the help of ANOVA test.

Step 5 Multi-objective optimization of squeeze casting process parameters to attain the optimal casting quality

The casting with minimum defects relies mainly on best set of different casting variables. No acceptable universal standards defined yet for such combinations of squeeze casting variables. There are many optimization tools currently available and each has distinct limitations and advantages. Based on the mapping model and the multi-objective problem-solving method, the data optimization software ISIGHT and NSGA-II algorithm was used to optimize the process parameters, and the approximate optimal solution was obtained from the global, so a more accurate and effective process parameter combination scheme was proposed.

Step 6 Validation of squeeze casting process based on actual casting experiments

The multi-objective optimization of the casting process parameters is carried out by means of the response surface method and intelligent optimization algorithms, thus determining the optimum combination of extrusion casting process parameters, and theoretically achieving a comprehensive optimization effect for virtual casting. Then, based on the actual casting test, the validity of the process scheme was verified by testing and analyzing the casting forming quality.

Experimental Details

Materials

An engineering automobile part (that is, gearbox body) made up of A356 alloy (Al–7Si–0.3Mg) was used as the casting material. Die material is the H13 die steels. The chemical compositions of the casting ingot and die materials are tested using optical emission spectrometer analysis and the results are presented in Table 2. The cooling system used water cooling.

The ambient temperature of the casting workshop is generally about 25°C, and the interface heat transfer coefficient between the die and the atmosphere is set as 10 W/(m²·K); There is a certain gap between the dies, so the heat between them is not equal. Set the interface heat transfer coefficient between the dies as 3000 W/(m²·K). The interfacial heat transfer coefficient between liquid metal and die is greatly affected by temperature and pressure. In this manuscript, the interface heat transfer coefficient between the metal liquid and the die changes with temperature as shown in Figure 3.

Criterion of Casting Defect Evaluation Indexes

Porosity

According to the formation mechanism of porosity, many researchers have put forward various criteria to predict porosity, including Niyama method, temperature gradient method and residual melt modulus criterion. Niyama criterion is the most popular one among these criteria. Although Niyama criterion can be better applied to the prediction of steel casting shrinkage porosity defect, but the crystallization temperature range wide, inspiratory tentatiousness of large aluminum alloy, due to the hydrogen content of the formation of shrinkage porosity defect and severe degree of influence over the influence of the casting solidification shrinkage, therefore its shrinkage prediction of shrinkage cavity defects in aluminum alloy has bigger error.^{29,30} The evaluation index proposed by Syvertsen and Freddy for predicting porosity defects in aluminum alloy castings was adopted in this paper. Based on the local

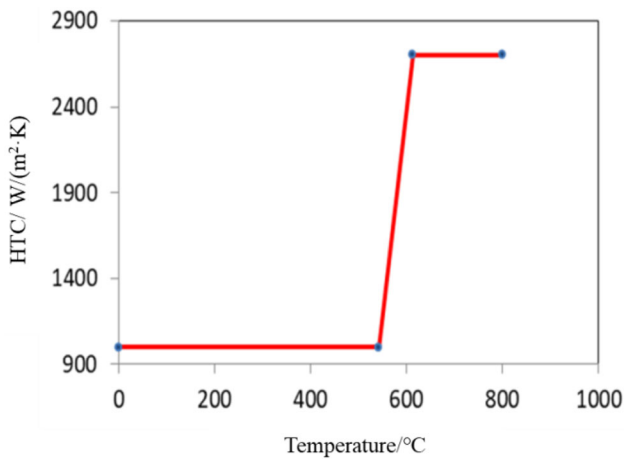


Figure 3. Heat transfer coefficient between liquid metal and die.

temperature gradient and cooling rate, the local solidification time is introduced. The criterion is represented below,^{28,31}

$$P = 0.325226 \left(\frac{G^2 \times t^{2/3}}{R} \right)^{-0.287531} \quad \text{Eqn. 1}$$

where P is the evaluation index of porosity defect of aluminum alloy; G is the local temperature gradient; t is local solidification time; R is the cooling rate. When the value is greater than or equal to 1, it is considered that shrinkage cavity and porosity defect will occur there.

Secondary Dendrite Arm Spacing

The secondary dendrite arm spacing (SDAS) can effectively reflect the mechanical properties of the casting. The smaller the spacing value is, the higher the density of the inner structure of the casting is, and the better the mechanical properties are. Furer–Wunderlin model was used to predict the secondary dendrite spacing of castings. The mathematical equation of the model is represented below,³²

$$\lambda = 5.5(A t_f)^{1/3} \quad \text{Eqn. 2}$$

where λ is the second dendritic spacing; t_f is local solidification time; A is the coarsening coefficient. Usually, when the aluminum alloy material and casting process are determined, the coarsening coefficient A can be treated as a constant, thus equation can be simplified as follows,

$$\lambda = B(t_f)^{1/3} \quad \text{Eqn. 3}$$

where B can be obtained by mathematical approximation method based on the experimental data of secondary dendrite spacing. For A356, when B is equal to 8.5, the distribution trend of SDAS value simulated curve is

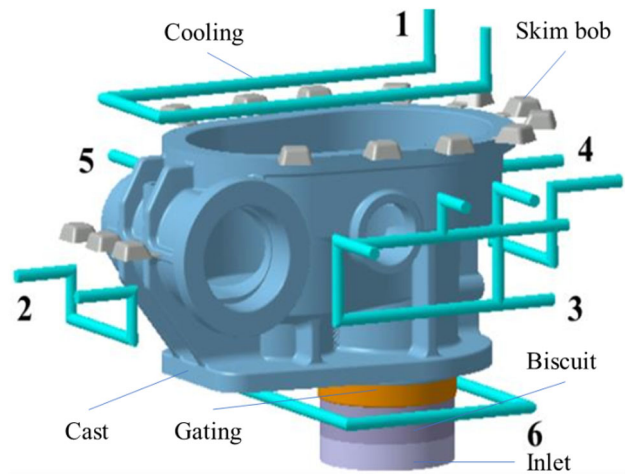


Figure 4. Schematic diagram of experimental system.

basically consistent with the measured curve, and the numerical agreement is relatively high.^{33,34}

Experimental System

The virtual casting test system includes mold, casting, pouring system and cooling system. Schematic diagram of experimental system is shown in Figures 4 and 5.

Process Parameters

Based on the determined casting structure, material, gating system, cooling lines, etc., the input variables and operating levels used for experimentation are presented in Table 3.

Experimental Details

Solidification of liquid metal under high pressure is one of the main advantages of squeeze casting. Generally speaking, the higher the specific pressure, the better the feeding effect of casting solidification, the higher the density of the internal structure, and the better mechanical properties and surface finish after forming. However, when the specific pressure increases to a certain value, the improvement of casting performance is very limited. It will cause the waste of power, increase the loss of mold and even produce parting surface flashing and other problems. Therefore, the specific pressure of the gearbox body squeeze casting is set as 100MPa.

In the squeeze casting process of gearbox body, the corresponding hot spot must be cooled to adjust the temperature difference between hot and cold spot, so as to ensure that the whole gearbox body has an ideal increasing temperature gradient after the filling of molten aluminum, and the molten aluminum can solidify in order in the mold.

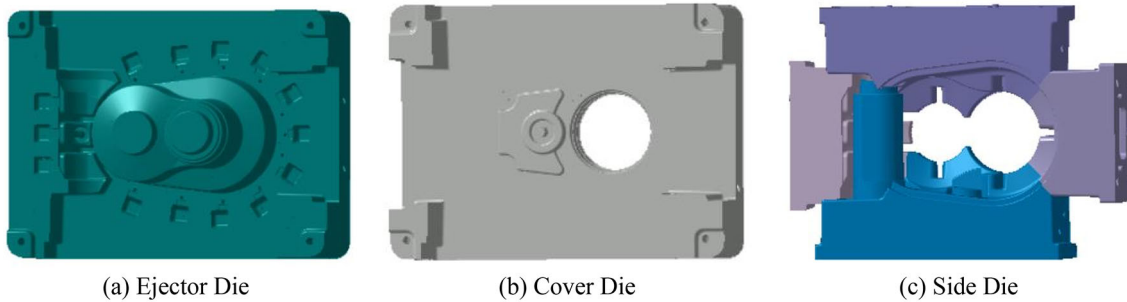


Figure 5. Scheme diagram for die.

Table 3. Squeeze Casting Parameters and Corresponding Levels

Process parameters	Coded notation	Uncoded notation	L-1	L-2	L-3
Pouring temperature, T_p [°C]	A	x_1	640	660	680
The first stage filling velocity, V_f [m/s]	B	x_2	0.1	0.15	0.2
The second stage filling velocity V_s [m/s]	C	x_3	0.2	0.25	0.3
Die temperature T_c [°C]	D	x_4	200	240	280

Table 4. Cooling Process Parameters of Cooling Tube

Number	Temperature	Flux (m^3/h)	Start time (s)	End time (s)
1	25	0.8	3.5	15
2	25	1	10	60
3	25	1	10	60
4	25	1	10	60
5	25	1	10	60
6	25	1.2	65	80

In order to enable the cooling system designed in Figure 4 to adjust the temperature field distribution of the gearbox body in the solidification process and make it solidify sequentially along the feeding path, parameters such as cooling water temperature and flow rate should be set in accordance with the solidification law of metal liquid from top to bottom from outside to inside, so as to achieve good cooling effect. Therefore, when other process parameters remain unchanged, the cooling process parameters finally set are shown in Table 4 after verification and comparison of numerical simulation calculation for many times.

According to the experiments arranged in Table 1, virtual casting experiments were conducted, respectively, to

Table 5. The Results of Evaluation Indexes

Exp. no.	Porosity (Y_1)	SDAS ($Y_2/\mu m$)	Solidification time (Y_3/s)
1	9.53	43.36	134.7
2	2.91	40.39	109.7
3	9.67	41.31	116.9
4	5.02	40.22	109.2
5	2.73	40.13	108.9
6	9.23	43.58	137.0
7	2.33	39.70	104.2
8	2.16	38.26	93.5
9	5.39	40.47	110.1
10	6.78	42.77	129.8
11	12.84	44.83	149.1
12	9.36	43.80	139.4
13	2.99	40.24	109.3
14	3.94	39.56	102.8
15	4.65	40.98	115.2
16	9.93	44.06	142.6
17	4.96	38.08	91.92
18	9.66	41.96	123.7
19	8.36	41.15	116.9
20	7.24	39.16	100.2
21	2.52	40.41	109.8
22	5.39	38.94	99.39
23	5.55	40.00	106.8
24	6.83	40.27	108.2
25	9.15	41.58	119.6
26	6.08	38.50	95.5
27	2.86	40.40	109.7
28	1.94	37.67	89.5
29	9.07	41.51	118.9

obtain experimental indexes such as solidification time, secondary dendrite spacing and value of porosity under different factor combinations.

Results and Discussion

In this section, the virtual casting optimization scheme was determined, followed by the discussion of mathematical model. The experimental input–output data had been collected as Box–Behnken design. The collected experimental data were utilized to develop nonlinear input–output relations. The input–output relationship was studied using response surface method (RSM). Performance of the developed model had been tested with the help of test cases and optimum process parameter setting was determined using data optimization software ISIGHT and NSGA-II.

The Determination of Virtual Casting Optimization Scheme

The 29 groups of experiment schemes in Table 1 were conducted for virtual casting, respectively. The results of solidification time, maximum secondary dendrite spacing (SDAS) and the maximum porosity of gearbox body under different combination of factors were obtained. The evaluation values of porosity and maximum secondary dendrite spacing of casting were calculated according to Eqns. 1 and 3. The results are listed in Table 5.

Response Surface Model Development of Porosity

Through the analysis of response surface test data, the second-order polynomial is used to fit the mapping relationship between Y_1 (criterion value of porosity) and various process parameters, and the second-order regression equation with porosity criterion value as the response index is shown in Eqn. 4.

$$\begin{aligned}
 Y_1 = & 2598.46342 - 7.15801x_1 - 570.32167x_2 \\
 & - 1023.425x_3 - 0.9337x_4 + 0.2725x_1x_2 + 0.785x_1x_3 \\
 & + 0.000237x_1x_4 + 515x_2x_3 + 0.003125x_2x_4 \\
 & + 0.47375x_3x_4 + 0.005301x_1^2 + 854.93333x_2^2 \\
 & + 596.68333x_3^2 + 0.001501x_4^2.
 \end{aligned}$$

Eqn. 4

After obtaining the fitting model of response index Y_1 (porosity criterion value), the validity of the model fitting should be verified first, and the statistical analysis results are shown in Table 6. P value can test the significance of the fitting model (P value > 0.05 means insignificant; $0.01 < P$ value < 0.05 indicates significant; P value < 0.01 indicates extreme success). The P value of the model is less than 0.0001 and P value of lack of fit is equal to 0.1371, which is more than 0.05, indicating that the model can well reflect the influence rule of the changes of various experimental factors on the response index. When the multiple correlation coefficient R^2 reaches 0.9952, means

Table 6. Statistical Analysis Results of the Fitting Model

Source	Value	Source	Value
P value of model	< 0.0001	P value of lack of fit	0.1371
Standard deviation	0.2945	R^2	0.9952
CV%	4.77	Adj. R^2	0.9905
Precision AP	49.68	Pre. R^2	0.9748

that 99.52% of the numerical change of Y_1 (criterion value of porosity) is caused by the change of experimental factors, and the coefficient of variation CV is 4.77%, which strongly verifies the validity of the fitting model.

The residual distribution of the model is shown in Figure 6a, from which it can be seen more intuitively that the residual basically conforms to normal distribution with fewer outliers. It can be seen from Figure 6b that the data results of the test and the predicted results of the model are basically distributed in a straight line, indicating that the model can well predict the test results of the response index Y_1 .

The influence of each experimental factor on the response index was visualized by response surface map generated by the fitting model. Response surface plots of each experimental factor to Y_1 are presented in Figure 7.

As shown in Figure 7a, the response surface plot reflects the influence trend of experimental factors A and B on response index Y_1 when experimental factors C and D are intermediate horizontal values. It can be seen from the figure that Y_1 (criterion value of porosity) increases with the increase in A (that is, pouring temperature). With the increase in B (that is, the velocity of the front filling section), it first decreases and then increases, indicating that the lower level interval of casting temperature below 660°C and the middle level interval of the velocity of the front filling section at about 0.15 m/s are conducive to reducing the shrinkage cavity defects of the gearbox body.

As shown in Figure 7b, the response surface plot reflects the influence trend of experimental factors A and C on response index Y_1 when experimental factors B and D are intermediate horizontal values. As can be seen, when the pouring temperature is in a low range, Y_1 decreases with the increase in the velocity of the second filling section. However, when the velocity increases to a certain extent, the change of the criterion value is not obvious. This indicates that properly accelerating the velocity at the end of filling can help to reduce the porosity.

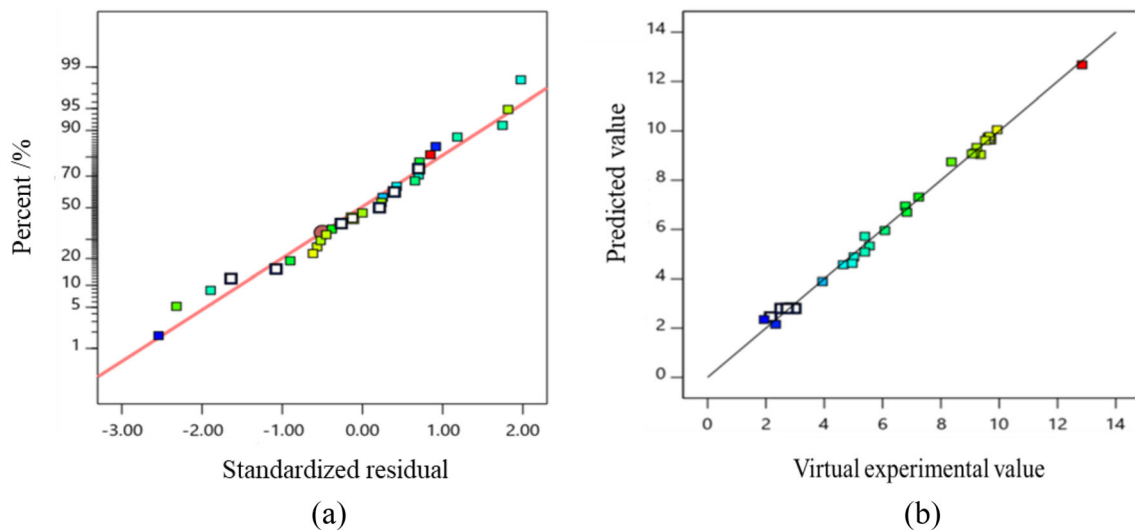


Figure 6. Residual distribution and data fitting diagram.

As shown in Figure 7c, the response surface plot reflects the influence trend of experimental factors A and D on response index Y_1 when experimental factors B and C are intermediate horizontal values. As can be seen, Y_1 reduces gradually with pouring temperature and die temperature gradually reducing. However, the change becomes insignificant after a certain degree of decrease. This shows that the forming quality of the casting can be effectively improved by choosing the appropriate low pouring temperature and die temperature for squeeze casting.

Similarly, according to Figure 7d–f, it can be found that when the velocity of the front part of mold filling is kept at about 0.15 m/s, the velocity of the back part is relatively fast and the preheating temperature of the mold is low, Y_1 is beneficial to decrease.

Response Surface Model Development of SDAS

Through the analysis of response surface test data, the second-order polynomial is used to fit the mapping relationship between Y_2 (SDAS) and various process parameters, and the second-order regression equation with SDAS as the response index is shown in Eqn. 5.

$$\begin{aligned}
 Y_2 = & 303.9798 - 0.7458x_1 - 40.76x_2 - 72.7x_3 - 0.224233x_4 \\
 & + 0.0025x_1x_2 + 0.0575x_1x_3 + 0.000178x_1x_4 - 3x_2x_3 \\
 & + 0.02x_2x_4 + 0.0025x_3x_4 + 0.000554x_1^2 + 93.2x_2^2 \\
 & + 65.2x_3^2 + 0.000353x_4^2.
 \end{aligned}$$

Eqn. 5

After obtaining the fitting model of response index Y_2 (SDAS), the validity of the model fitting should also be verified. The statistical analysis results are shown in Table 7. The P value of model is less than 0.0001 in the

table, and the P value of lack of fit is equal to 0.9822, which is more than 0.05, indicating that the model can well reflect the influence rule of the changes of various test factors on the response index. When the multiple correlation coefficient reaches 0.999, 99.9% of the numerical change of Y_2 is caused by the change of experimental factors, and the coefficient of variation is 0.1993%, which strongly verifies the validity of the fitting model.

Model of residual distribution as shown in Figure 8a, the secondary dendrite arm spacing of model test value compared with the predicted values as shown in Figure 8b, also can see the residual basic accord with normal distribution, distribution of basic experimental and predicted values on a straight line, show that the model can be very good for Y_2 response index (SDAS) for predicting the experimental results.

The influence of each experimental factor on the response index was visualized by response surface map generated by the fitting model. Response surface plots of each experimental factor to Y_2 are presented in Figure 9.

As shown in Figure 9a, the response surface plot reflects the influence trend of experimental factors A and B on response index Y_2 when experimental factors C and D are intermediate horizontal values. As can be seen, the surface is quite flat and has no obvious ups and downs, Y_2 has a slight upward tendency with the increase in pouring temperature. However, with the change of the velocity of the first filling section, there is almost no change. This indicates that the increase in pouring temperature extends the local solidification time of the casting to a certain extent, leading to the increase in secondary dendrite arm spacing, while the change of velocity at the front of mold filling has

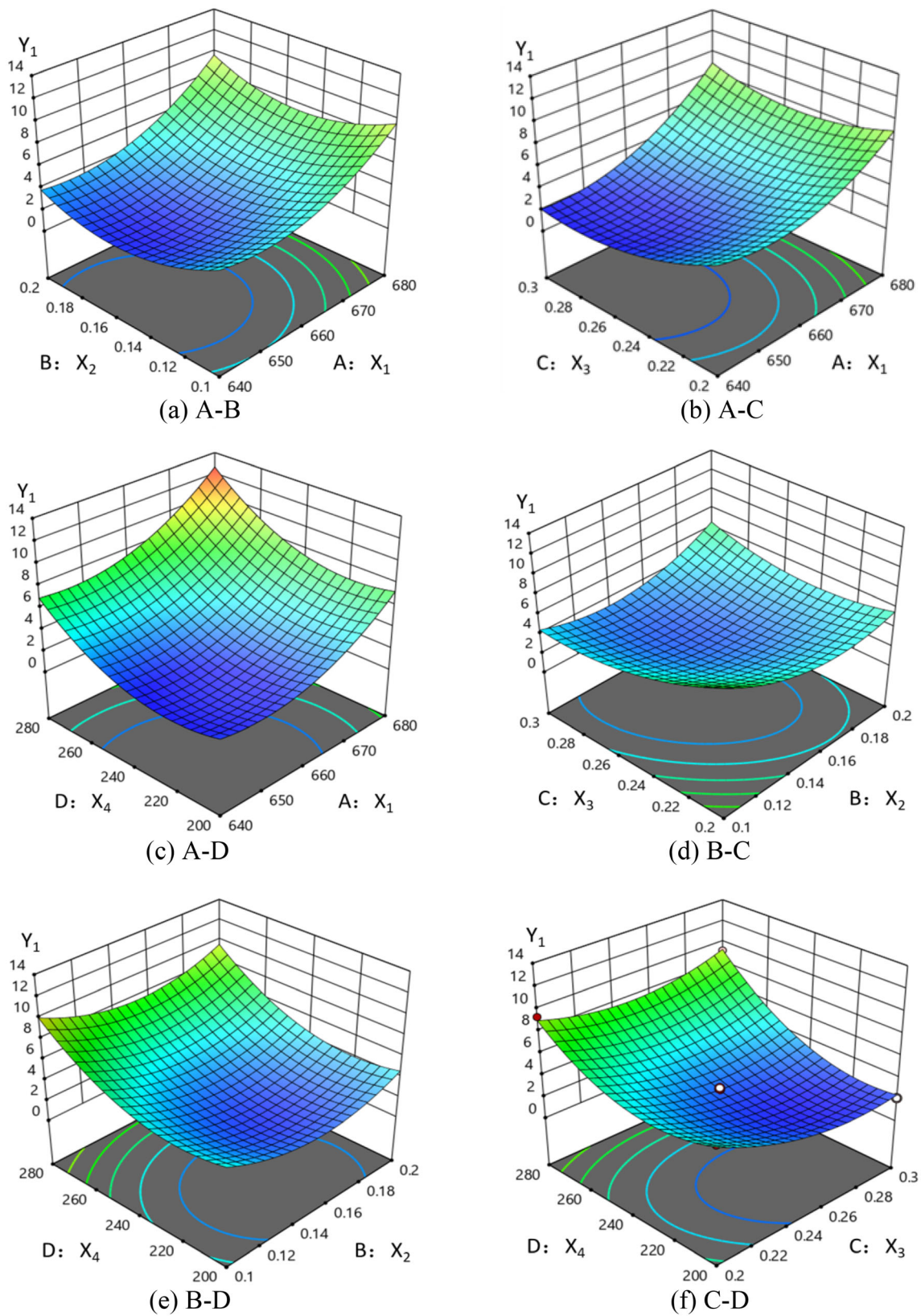


Figure 7. Response surface plots of each experimental factor to Y_1 .

little influence on the secondary dendrite arm spacing (SDAS).

As shown in Figure 9b, the response surface plot reflects the influence trend of experimental factors A and C on response index Y_2 when experimental factors B and D are

Table 7. Statistical Analysis Results of the Fitting Model

Source	Value	Source	Value
P value of model	< 0.0001	P value of lack of fit	0.9822
Standard deviation	0.0813	R^2	0.9990
CV%	0.1993	Adj. R^2	0.9981
Precision AP	120.3177	Pre. R^2	0.9972

intermediate horizontal values. As can be seen, the surface is also flat, and the change of the velocity of the second filling section has no obvious influence on Y_2 (SDAS).

As shown in Figure 9c, the response surface plot reflects the influence trend of experimental factors A and D on response index Y_2 when experimental factors B and C are intermediate horizontal values. As can be seen, the surface is steep and Y_2 increases with the increase in die temperature. This indicates that too high die temperature is not conducive to reducing the secondary dendrite arm spacing of castings.

Similarly, by Figure 9d–f can be seen that the die temperature on the casting secondary dendrite arm spacing is most significantly, the influence of because of casting solidification process is mainly between metal and mold heat exchange process, through the response surface analysis found that the appropriate die temperature, reducing to improve the mechanical properties of castings.

Response Surface Model Development of Solidification Time

Through the analysis of response surface test data, the second-order polynomial is used to fit the mapping relationship between Y_3 (Solidification time) and various process parameters, and the second-order regression equation with solidification time as the response index is shown in Eqn. 6.

$$\begin{aligned}
 Y_3 = & 2458.01417 - 6.32842x_1 - 216.66667x_2 - 542.26667x_3 \\
 & - 2.93787x_4 - 0.1x_1x_2 + 0.475x_1x_3 + 0.002681x_1x_4 - 20x_2x_3 \\
 & - 0.05375x_2x_4 - 0.05125x_3x_4 + 0.0045x_1^2 + 766.5x_2^2 \\
 & + 450.5x_3^2 + 0.003617x_4^2.
 \end{aligned}$$

Eqn. 6

After obtaining the fitting model of response index Y_3 (solidification time), the validity of the model fitting should also be verified. The test data are shown in Table 8. The P value of model is less than 0.0001 in the table, and the P value of lack of fit is equal to 0.2488, which is more than 0.05, indicating that the model can well reflect the influence rule of the changes of various test factors on the response index. When the multiple correlation coefficient reaches 0.9995, it indicates that 99.95% of the variation in the value of Y_3 (solidification time) is due to changes in experimental factors and the coefficient of variation is 0.4413%, which strongly verifies the validity of the fitting model.

The residual distribution of the model is shown in Figure 10a, and the comparison between the model test value and predicted value of solidification time is shown in Figure 10b. It can also be seen that the residual basically conforms to normal distribution, and the test value and predicted value are basically distributed in a straight line,

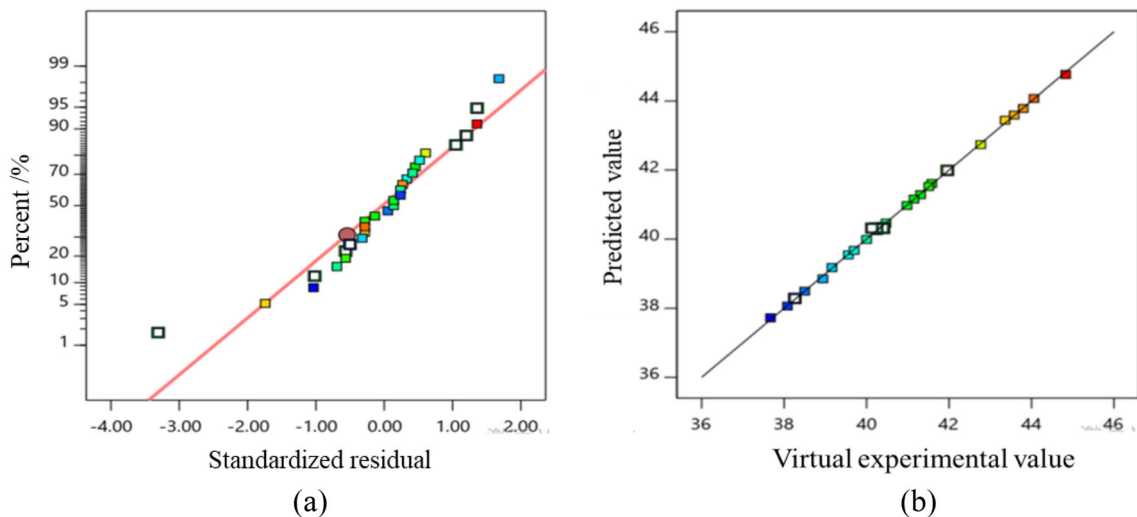


Figure 8. Residual distribution and data fitting diagram.

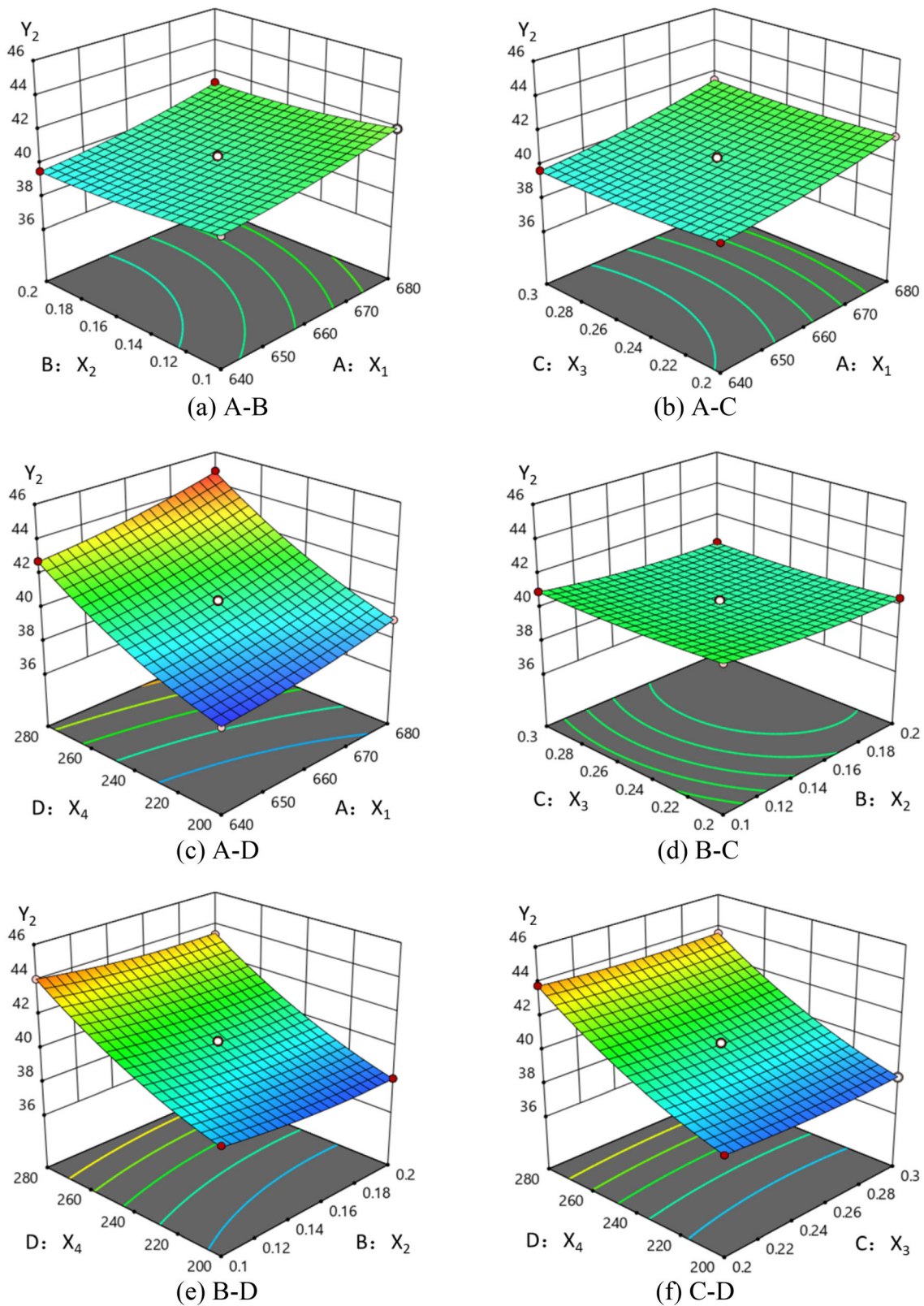


Figure 9. Response surface diagram of each experimental factor to Y_2 .

indicating that the model can well predict the experimental results of response index Y_3 (solidification time).

The influence of each experimental factor on the response index was visualized by response surface map generated by the fitting model. Response surface plots of each experimental factor to Y_3 are presented in Figure 11.

Table 8. Statistical Analysis Results of the Fitting Model

Source	Value	Source	Value
P value of model	< 0.0001	P value of lack of fit	0.2488
Standard deviation	0.5026	R^2	0.9995
CV%	0.4413	Adj. R^2	0.9990
Precision AP	160.8135	Pre. R^2	0.9973

As shown in Figure 11a, the response surface plot reflects the influence trend of experimental factors A and B on response index Y_3 when experimental factors C and D are intermediate horizontal values. As can be seen, Y_3 increases with the increase in pouring temperature, but the amplitude is relatively gentle. However, the change of the filling velocity at first stage has no obvious influence on the surface tendency, indicating that the influence of pouring temperature on solidification time is more significant than that of the filling velocity.

Similarly, it can be seen from Figure 11b and d that the surface has no obvious fluctuation with the change of the filling velocity, indicating that the filling velocity has no significant influence on the length of solidification time of casting. However, it can be seen from Figure 11c, e and f that the surface changes sharply. Y_3 (solidification time) increases obviously with the increase in die temperature, indicating that higher die temperature is not conducive to heat loss of metal liquid, resulting in longer solidification time.

Multi-objective Optimization of Process Parameters

In engineering applications, it is often necessary to optimize multiple objective variables. In addition, different target variables are likely to conflict with each other. For example, the optimization of one indicator may lead to other indicators being far away from the optimization direction, and it is difficult to achieve the ideal situation where all objectives are simultaneously optimal. Therefore, it is necessary to balance and coordinate among multiple objectives to achieve the comprehensive optimal effect.³⁵

In order to ensure the casting forming quality and take into account the production efficiency and economy, it is necessary to optimize the shrinkage cavity, secondary dendrite spacing and solidification time at the same time. Data optimization software ISIGHT and NSGA-II algorithm are applied to the optimization.

Establishment of Multi-objective Optimization Model

Through the analysis of the test results of the response surface of section 4.1 of this chapter, respectively, obtained the response index Y_1 (criterion value of porosity), Y_2 (secondary dendrite arm spacing), Y_3 (solidification time), respectively, and the casting process parameters A (pouring temperature) and B (filling the front speed), C (after filling speed), D (die temperature) between the quadratic response surface regression equation. In order to effectively guide the actual production, it is necessary to keep all process parameters within a reasonable range of variation, so that the values of Y_1 , Y_2 and Y_3 are as small as possible. In other words, the optimization objectives of these three

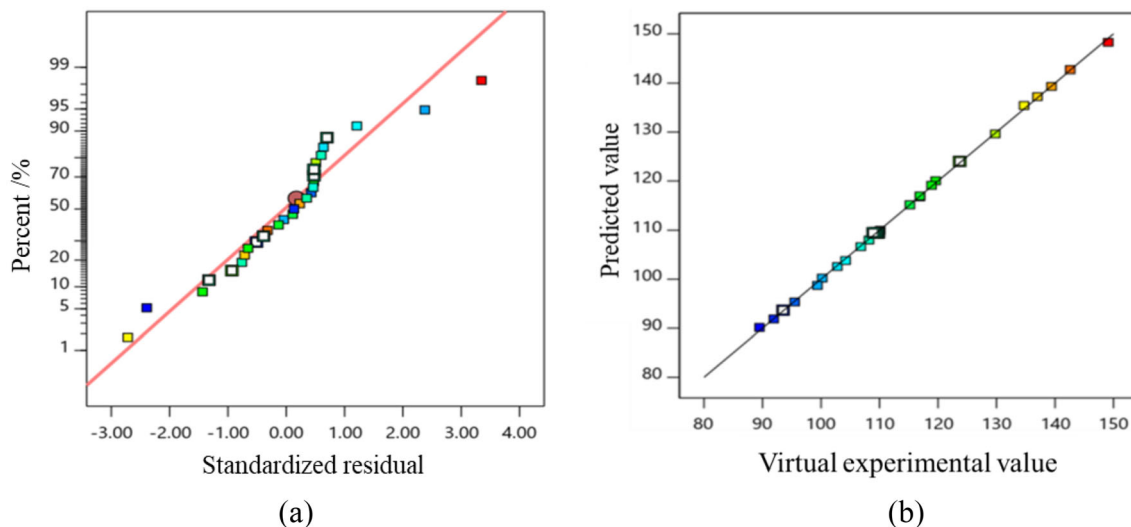


Figure 10. Residual distribution and data fitting diagram.

objectives have been defined and can be expressed as follows:

$$\begin{aligned} \text{Min : } Y_1 = & 2598.46342 - 7.15801x_1 - 570.32167x_2 - 1023.425x_3 \\ & - 0.9337x_4 + 0.2725x_1x_2 + 0.785x_1x_3 + 0.000237x_1x_4 + 515x_2x_3 \\ & + 0.003125x_2x_4 + 0.47375x_3x_4 + 0.005301x_1^2 + 854.93333x_2^2 \\ & + 596.68333x_3^2 + 0.001501x_4^2 \end{aligned}$$

Eqn. 7

$$\begin{aligned} \text{Min : } Y_2 = & 303.97975 - 0.745817x_1 - 40.76x_2 - 72.7x_3 - 0.224233x_4 \\ & + 0.0025x_1x_2 + 0.0575x_1x_3 + 0.000178x_1x_4 - 3x_2x_3 \\ & + 0.02x_2x_4 + 0.0025x_3x_4 + 0.000554x_1^2 + 93.2x_2^2 \\ & + 65.2x_3^2 + 0.000353x_4^2 \end{aligned}$$

Eqn. 8

$$\begin{aligned} \text{Min : } Y_3 = & 2458.01417 - 6.32842x_1 - 216.66667x_2 - 542.26667x_3 \\ & - 2.93787x_4 - 0.1x_1x_2 + 0.475x_1x_3 + 0.002681x_1x_4 - 20x_2x_3 \\ & - 0.05375x_2x_4 - 0.05125x_3x_4 + 0.0045x_1^2 + 766.5x_2^2 \\ & + 450.5x_3^2 + 0.003617x_4^2 \end{aligned}$$

Eqn. 9

$$640 \leq x_1 \leq 680; 0.1 \leq x_2 \leq 0.2; 0.2 \leq x_3 \leq 0.3; 200 \leq x_4 \leq 280.$$

Eqn. 10

The pouring temperature, the filling velocity at the first and second stage and the mold preheating temperature are set as the design variables. Y_1 , Y_2 and Y_3 are selected as the target variables. The optimization direction is minimized, and the NSGA-II algorithm is selected for optimization. The mapping relationship between input and output data of workflow is shown in Figure 12.

Analysis of Optimization Results

Due to the simultaneous optimization of three target variables, there will be conflicts between different variables in the process, that is, the optimization of one target quantity may cause other target quantities to deviate from the optimization direction, so the final result is not a single optimal solution, but a Pareto solution set containing many solutions. After multi-objective optimization of the criterion value of porosity, secondary dendrite arm spacing and solidification time through the algorithm, part of the solution set is shown in Table 9.

From the optimization solution in Table 9, it can be found that the process parameters have certain regularity: pouring temperature is at 645°C or so float; The filling velocity at the first stage remains at about 0.15; The filling velocity at the second stage remains at about 0.28; and the die temperature is at 210°C or so float. The parameter distribution is also consistent with the paper on the response surface analysis results.

In actual production, the pouring temperature of liquid metal is controlled by a holding furnace, filling speed is determined by the injection speed of the punch and die temperature is controlled by the die temperature machine,

considering the various process parameters setting accuracy is limited, so choose the near optimal solution set of integer as the final process parameters combination, namely the pouring temperature is 645°C; filling velocity at the first stage is 0.15m/s; filling velocity at the second stage is 0.28m/s; and the mold preheating temperature is 210°C.

Numerical Simulation Verification of Optimal Process Parameters

Based on the optimal process parameters selected after multi-objective optimization, numerical simulation was carried out to verify the effectiveness of the optimization under the condition that other process parameters remained unchanged. Figure 13 shows the distribution results of shrinkage cavity and porosity and secondary dendrite arm spacing under the final process scheme.

As can be seen from Figure 13, there is basically no porosity defect in the casting, and the secondary dendrite spacing is 38.09 micron, indicating that the density of the internal microstructure is improved. In addition, the solidification time under this process is 92.91s, indicating that the production cycle is also shortened. Therefore, from the point of view of virtual casting, the casting forming quality and production efficiency are further improved by multi-objective optimization, and the comprehensive optimal effect is achieved.

Squeeze Casting Verification Experiments

The multi-objective optimization of squeeze casting process parameters based on response surface method in Sections 4.1 and 4.2 theoretically achieves the comprehensive optimal effect from the perspective of virtual casting experiments. Based on actual production trial production, this section verifies the validity of the process scheme by testing and analyzing the forming quality of aluminum alloy gearbox.

Forming Experiments

The process steps of squeeze casting test of gearbox are summarized in Figure 14.

In order to accurately control the pouring temperature, the high-temperature molten metal obtained by smelting is placed in a holding furnace through a flow bag, and the temperature is set at 645°C. Mold temperature is controlled to 210°C by mold temperature machine. After the mold temperature is stable, spray release agent evenly on the surface of the mold, especially for the inner gate and complex cavity structure and other parts prone to stick mold can be more appropriate.

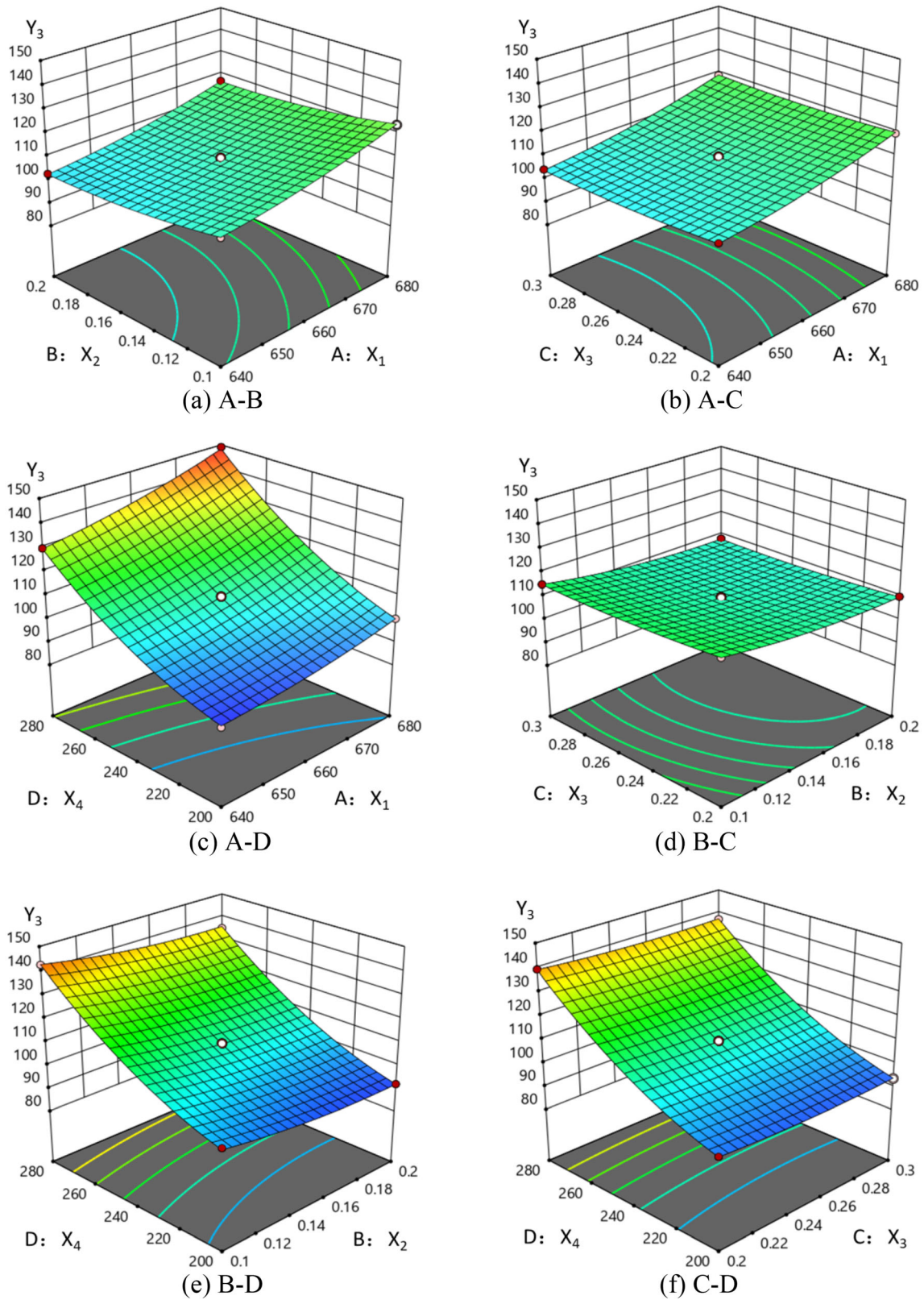


Figure 11. Response surface diagram of each experimental factor to Y_3 .

After the mold is locked, the soup feeder will inject the metal liquid into the inclined chamber from the holding furnace. At this time, the chamber is rising directly to the

feed port to complete the docking. The front velocity of the punch is set at 0.15m/s, and the filling lasts for 1.8s smoothly. The velocity rises to 0.28m/s when the cavity is

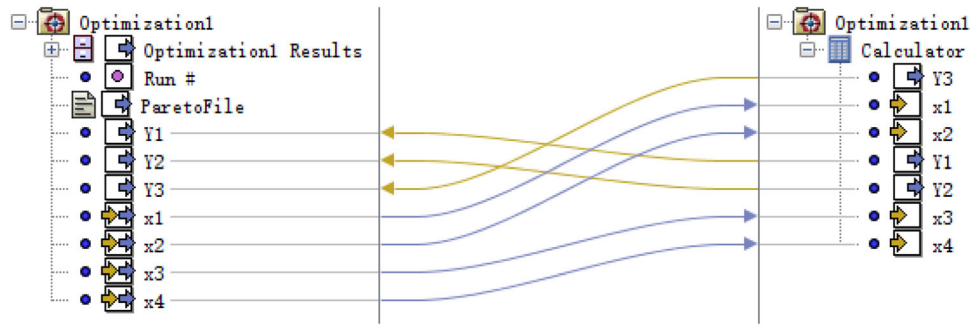
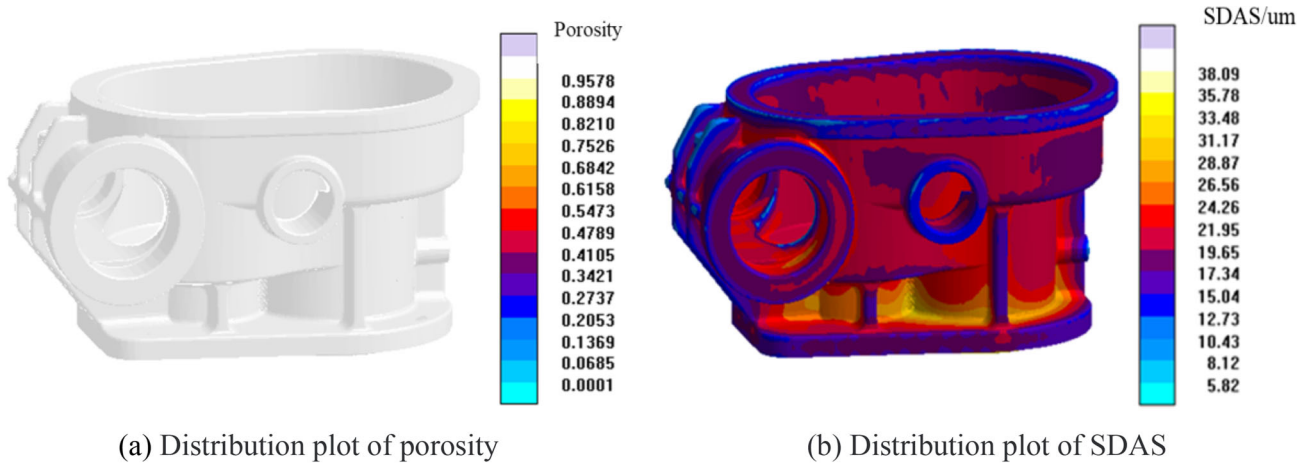


Figure 12. Input and output data mapping diagram.

Table 9. Multi-objective Optimization Part Pareto Optimization Solution Set

No.	$x_1/^\circ\text{C}$	$x_2/\text{m/s}$	$x_3/\text{m/s}$	$x_4/^\circ\text{C}$	Y_1	$Y_2/\mu\text{m}$	Y_3/s
1	644.25	0.150	0.267	208.19	0.9818	37.92	92.21
2	644.34	0.143	0.273	205.42	0.9680	37.86	91.94
3	644.65	0.145	0.268	209.34	0.9530	38.01	92.93
4	644.59	0.143	0.284	213.05	0.6781	38.19	94.14
5	645.69	0.149	0.284	213.05	0.6929	38.16	93.84
6	646.35	0.151	0.284	213.05	0.7084	38.17	93.87
7	643.67	0.143	0.286	209.88	0.7205	38.04	93.09
8	644.65	0.143	0.294	208.26	0.7418	38.01	92.87
9	644.30	0.145	0.295	208.01	0.7602	37.98	92.60
10	643.63	0.143	0.282	208.26	0.7755	37.97	92.60



(a) Distribution plot of porosity

(b) Distribution plot of SDAS

Figure 13. The casting quality after optimization.

about 60% full until the filling is completed. Continuous pressure on the punch ensures that the casting is fully fed under high pressure, and the pressure is kept until it is completely solidified. Then the pressure chamber returns to the original tilt position and waits for the next working cycle to open the mold and take parts.

The casting taken out of the mold contains the gating system. First observe whether the gearbox is insufficient pouring, cold isolation and deformation. The casting system shall be removed after the visual inspection is qualified.

The T6 heat treatment process was conducted according to the casting material and performance requirements. The solution treatment is at 530°C for 4 hours, and the aging

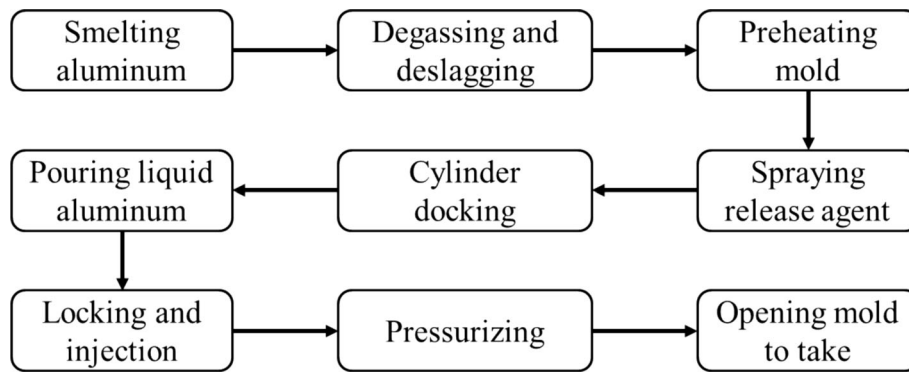


Figure 14. Squeeze casting test process of gearbox.



Figure 15. XG-160T/C type detector.

treatment is at 160°C for 6 hours. In addition, the aluminum alloy gearbox with good surface quality and high-dimensional accuracy was obtained by finishing processing.

X-ray Testing

In order to directly judge the forming quality inside the casting, X-ray is used to detect the internal defects of aluminum alloy gearbox. The equipment adopts XG-160T/C detector, as shown in Figure 15, mainly to detect the complex changes of box structure and local thicknesses prone to shrinkage cavity defects, as shown in Figure 16.

Place the aluminum alloy gearbox on the test table at an appropriate angle. The defects of porosity in casting can be detected directly by using the testing instrument. As can be seen from the test results in Figure 17, under the optimal process scheme determined in this manuscript, all parts of the box body can get good feeding, so the forming quality is high.



Figure 16. Detection position diagram

Metallographic Structure Testing

In order to test the distribution of microstructure inside the casting, the metallographic structure was observed. Selecting the right position for sampling can more objectively and comprehensively reflect the forming quality of the casting. For the aluminum alloy gearbox, the metallographic sample is selected at the position that is closest to its average performance and can reflect different filling and solidification stages, as shown in Figure 18.

The sample size is about 15*15*15mm, and a relatively flat surface is selected for polishing until there is no obvious cutting fracture on the surface. After etching with 5% HF acid for about 30 seconds, the surface appears pale gray blue. At this time, rinse with alcohol and blow dry to avoid direct contact with hands. The metallographic structure was observed under microscope with a tweezers, as shown in Figure 19.

It can be seen from the figure that the microstructure is mainly composed of α -Al matrix and eutectic Si phase distributed at grain boundaries. The dendrite morphology is

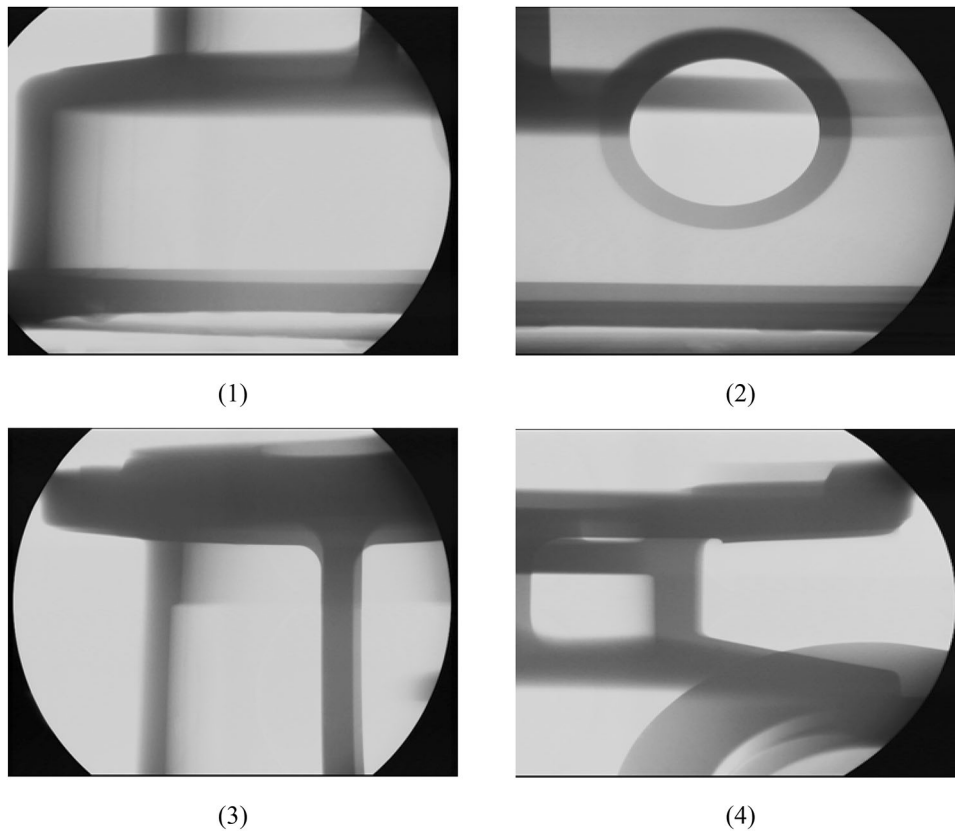


Figure 17. The testing results of the four position.

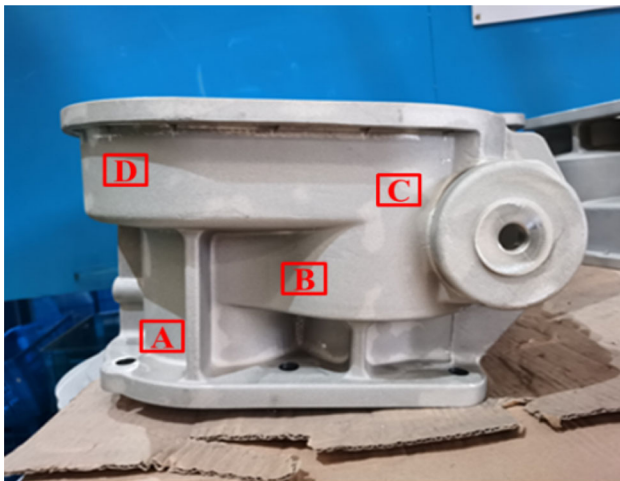


Figure 18. Sampling position diagram.

similar at different locations, the size and thickness of dendrite arms are basically the same, and the proportion of α -Al matrix and eutectic components is roughly the same, indicating that the microstructure of different locations of the casting is consistent. The samples of position A and B are closest to the flow gate and have the smallest pressure transfer loss and the largest extrusion pressure in the process of pressurized solidification. Therefore, the microstructure there is the densest and the grain size is small. In addition, although there are some pores in

samples B and C, there is no obvious porosity defect, which will not affect the mechanical properties of the casting within the acceptable range.

Mechanics Performance Testing

In order to test the mechanical properties of aluminum alloy gearbox, tensile properties and hardness tests were carried out on it. Similarly, the correct sampling position could comprehensively reflect the mechanical properties of different parts of the box, and sampling was carried out in the relatively flat position of the box with little change in wall thickness, as shown in Figure 20.

Two tensile samples were taken from each corresponding position marked in Figure 20. The equipment used WDW-100 universal tensile testing machine, and the tensile rate was set at 0.1mm/min. Two hardness test samples were taken in the same position, and the equipment adopted Richter digital hardness tester. The test load was set at 100kgf for 5s, and the test average value of all samples was finally calculated as the basis for measuring the mechanical properties of aluminum alloy gearbox. The test results are shown in Table 10.

According to the results in the table, the average tensile strength is 280.8MPa; the average elongation was 9.5%;

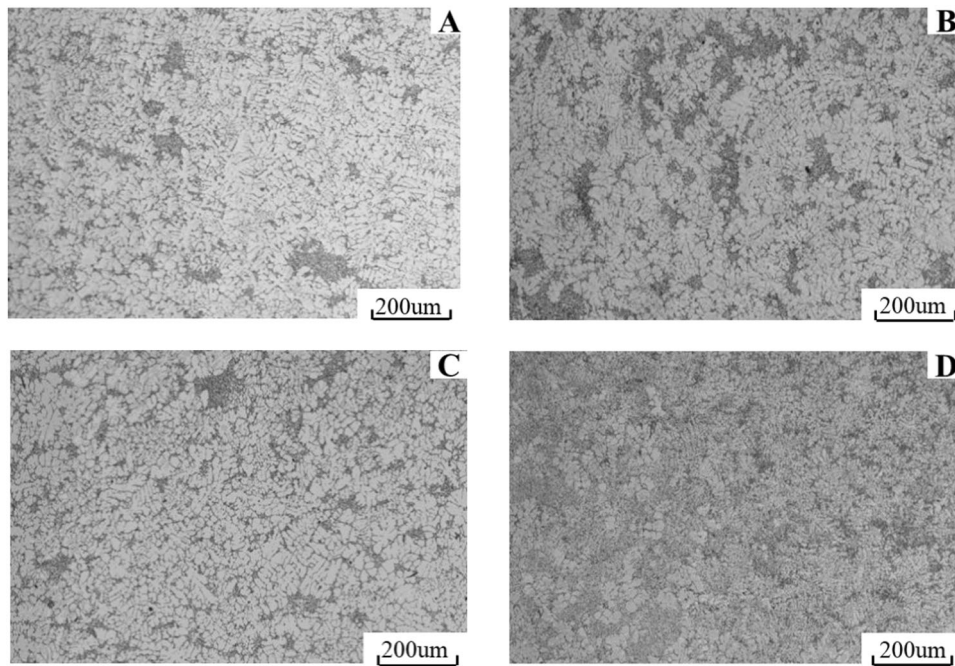


Figure 19. Metallographic structure diagram of different positions.

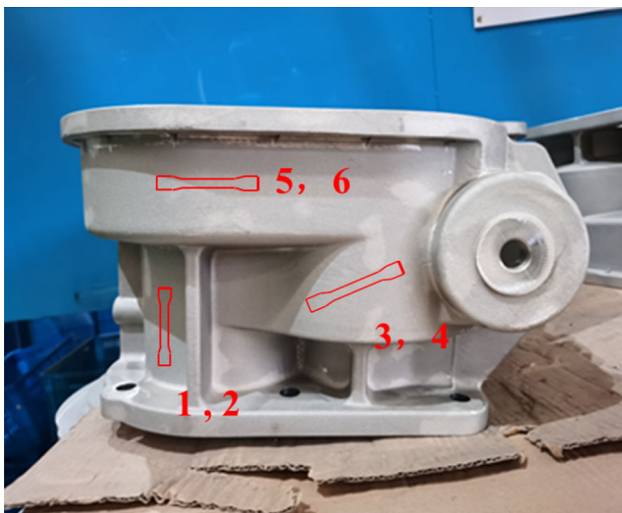


Figure 20. Sampling position diagram.

the average hardness is 91.2HBW. The test results meet the technical requirements of aluminum alloy gearbox. It can also be seen from Table 10 that the tensile strength, elongation and hardness values of samples at different sampling positions fluctuate within a very small range and are all higher than the technical requirements of parts with a certain margin, indicating that the mechanical properties of each part of the aluminum alloy gearbox are good and evenly distributed.

Conclusions

The defects of casting parts were modeled in squeeze process by using the statistical design of experiments and

Table 10. Test Results of Mechanical Properties of Aluminum Alloy Gearbox

No.	Tensile strength/ MPa	Tensile elongation/ %	Hardness/ HBW
1	280	9.3	91
2	286	9.1	94
3	281	9.1	94
4	281	9.7	90
5	278	9.8	89
6	279	9.5	91

soft computing-based approaches. The virtual casting experiments have been conducted and defects data were collected for the different squeeze casting conditions with RSM-BBD. The regression equation established can be used to predict the porosity rate, SDAS and solidification time of the target casting. NSGA-II algorithm optimization technique had been utilized to determine the optimum process variables corresponding to minimum defects combining with the data optimization software ISIGHT. The nonlinear mapping model can greatly improve the calculation efficiency under the condition of meeting the prediction accuracy and provide a good calculation basis for the optimization of process parameters. Further, it will help foundry men to know the more influencing process parameters in the squeeze process. The actual production casting with X-ray inspection, Metallographic structure testing and Mechanics performance testing experiments are

conducted to verify the optimization results. The two-stage optimization approach determines the optimal process scheme and can shorten the product development cycle, save cost and ensure the quality of castings, which is of great significance to guiding the production.

Acknowledgement

This work was supported by Jiangsu Postdoctoral Research Foundation (Grant No. 2020Z410), Jiangsu Industry and University Cooperation Project (Grant No. BY2019006), General Project of Natural Science Research in Universities of Jiangsu Province (Grant No. 19KJB460005) and Science and Technology Research Project of Hubei Provincial Department of Education (Grant No. Q20212602).

Conflict of Interest The authors declare that they have no known competing financial interests or personal relationships that could have appeared to influence the work reported in this paper.

REFERENCES

1. N. Yamamoto, M. Itamura, T. Ueno, Effects of squeeze casting on mechanical properties of aluminum die casting alloy. *Trans. Am. Foundrymen's Society* **100**, 539–546 (1992)
2. S. Okada, N. Fujii, A. Goto, S. Morimoto, T. Yasuda, Development of a full-automatic squeeze casting machine. *Trans. Am. Foundrymen's Society* **90**, 135–146 (1982)
3. N. Yamamoto, N. Kawagoishi, Fatigue characteristics of large squeeze cast aluminum wheel. *Trans. Am. Foundrymen's Society* **108**, 113–118 (2000)
4. M. Kim, J. Hwang, H. Kwon, Effect of squeeze cast process parameters on fluidity of Al-Si alloy. *Trans. Am. Foundrymen's Society* **114**, 59–70 (2006)
5. C. Lin, S. Wu, S. Lue et al., Effects of high pressure rheo-squeeze casting on Fe-containing intermetallic compounds and mechanical properties of Al-17Si-2Fe-(0, 0.8) V alloys. *Mater. Sci. Eng. A* **713**, 105–111 (2017)
6. J. Maj, W. Węglewski, K. Bochenek et al., A comparative study of mechanical properties, thermal conductivity, residual stresses, and wear resistance of Aluminum-Alumina composites obtained by squeeze casting and powder metallurgy. *Metall. Mater. Trans. A* **52**, 4727–4736 (2021)
7. J. Hao, H. Luo, J. Bian et al., The effect of squeeze casting process on the microstructure, mechanical properties and wear properties of hypereutectic Al-Si-Cu-Mg alloy. *Inter. Metalcast.* **16**, 153–165 (2022). <https://doi.org/10.1007/s40962-021-00575-x>
8. T. Vossel, N. Wolff, B. Pustal, A. Bhrig-Polaczek, Influence of die temperature control on solidification and the casting process. *Int. J. Metalcasting.* **14**, 907–925 (2020). <https://doi.org/10.1007/s40962-019-00391-4>
9. M. Arulraj, P.K. Palani, Parametric optimization for improving impact strength of squeeze cast of hybrid metal matrix (LM24-SiCp-coconut shell ash) composite. *J. Braz. Soc. Mech. Sci. Eng.* **40**(1), 2 (2018)
10. M.H. Sarfraz, M. Jahanzaib, W. Ahmed et al., Multi-response parametric optimization of squeeze casting process for fabricating Al 6061-SiC composite. *Int. J. Adv. Manufact. Technol.* **102**, 759–773 (2019)
11. M.T. Azhagan, B. Mohan, Parametric optimization in squeeze casting of AA6061-Si3N4 composites using Taguchi method. *J. Ceram. Process. Res.* **22**(4), 470–474 (2021)
12. S.A. Hassasi, M. Abbasi, S.J. Hosseinipour, Parametric investigation of squeeze casting process on the microstructure characteristics and mechanical properties of A390 aluminum alloy. *Int. J. Metalcast.* **14**(1), 69–83 (2020). <https://doi.org/10.1007/s40962-019-00325-0>
13. S.A. Hassasi, M. Abbasi, S.J. Hosseinipour, Effect of squeeze casting parameters on the wear properties of A390 Aluminum Alloy. *Int. J. Metalcast.* **15**(3), 852–863 (2021). <https://doi.org/10.1007/s40962-020-00507-1>
14. P. Krishna, K.T. Bilkey, R.D. Pehlke, Estimation of interfacial heat transfer coefficient in indirect squeeze casting. *Trans. Am. Foundry Society* **109**, 1–9 (2001)
15. Y. Li, H. Yang, Z. Xing, Numerical simulation and process optimization of squeeze casting process of an automobile control arm. *Int. J. Adv. Manuf. Technol.* **88**, 1–4 (2017)
16. Q.Y. Hu, H.D. Zhao, H. Long et al., Numerical simulation of mold filling and particulate flow of A356/SiCp indirect squeeze casting. *J. Compos. Mater.* **54**(12), 1593–1602 (2020)
17. H. Sanil, T.K. Deepak, M. Ravi, Experimental and numerical evaluation of squeeze cast Al-Si-Cu-Ni-Mg alloy for piston applications. *Mater. Manufact. Process.* **37**, 1145–1155 (2022)
18. Li J, Sun Y, Wang Y, et al. Optimization of squeeze casting process of gearbox cover based on FEM and Box-Behnken design (2022)
19. F. Pan, C. Steve, M. Daan et al., Examination and simulation of Silicon Macroseggregation in A356 wheel casting. *Metals-Open Access Metall. J.* **8**(7), 503 (2018)
20. P. Borlepwar, S. Biradar, Study on reduction in shrinkage defects in HPDC component by optimization of localized squeezing process. *Int. J. Metalcast.* **13**, 915–922 (2019). <https://doi.org/10.1007/s40962-018-00295-9>
21. P. Fan, S.L. Cockcroft, D.M. Maijer et al., Porosity prediction in A356 wheel casting. *Metall. Mater. Trans. B.* **50**(5), 2421–2435 (2019)
22. D. Sui, Z. Cui, R. Wang et al., Effect of cooling process on porosity in the Aluminum alloy automotive

- wheel during low-pressure die casting. *Int. J. Metalcast.* **10**, 32–42 (2016). <https://doi.org/10.1007/s40962-015-0008-0>
23. H. Yavuz, O. Ertugrul, Numerical analysis of the cooling system performance and effectiveness in Aluminum low-pressure die casting. *Inter Metalcast* **15**, 216–228 (2021). <https://doi.org/10.1007/s40962-020-00446-x>
 24. G. Ruff, T.E. Prucha, J. Barry, D. Patterson, Pressure counter pressure casting (PCPC) for automotive aluminum structural components. *SAE Trans.* **110**, 360–365 (2001)
 25. G.C.M. Patel, P. Krishna, M.B. Parappagoudar, Modeling of squeeze casting process using design of experiments and response surface methodology. *Int. J. Cast Metals. Res.* **28**, 167–180 (2015)
 26. P.G.C. Manjunath, P. Krishna, M.B. Parappagoudar, An intelligent system for squeeze casting process-soft computing based approach. *Int. J. Adv. Manuf. Technol.* **86**(9–12), 1–15 (2016)
 27. P.G.C. Manjunath, A.K. Shettigar, M.B. Parappagoudar, A systematic approach to model and optimize wear behaviour of castings produced by squeeze casting process. *J. Manuf. Process.* **32**, 199–212 (2018)
 28. P. Fan, S.L. Cockcroft, D.M. Maijer et al., Porosity prediction in A356 wheel casting. *Metall. Mater. Trans. B.* **50**(5), 2421–2435 (2019)
 29. J.A. Spittle, M. Almeshhedani, S.G.R. Brown, The Niyama function and its proposed application to micro-porosity prediction. *Cast Metals.* **7**(1), 51–56 (2019)
 30. F. Chiesa, J. Mammen, L.F. Smiley, Use of solidification modeling to predict porosity distribution in Al A356 industrial castings. *AFS Trans.* **106**, 98–68 (1998)
 31. Pequet CH, Rappaz M. Modeling of porosity formation during the solidification of aluminium alloys using a mushy zone refinement method. *Modeling of Casting, Welding and Advanced Solidification Processes IX*. Aachen, Germany. 71-79 (2000)
 32. Feurer U, Wunderlin R. *Metal Solidification*. Stuttgart: DGM Fachber. (1977)
 33. F. Chiesa, J. Mammen, L.F. Smiley, Use of solidification modeling to predict porosity distribution in Al A356 industrial castings. *AFS Trans.* **106**, 98–68 (1998)
 34. Li D, Li H, Xu H, et al. Research on the secondary dendrite arm spacing of aluminum alloy cylinder head based on MAGMA software. *Green Foundry and Sustainable Development - (25th) Chongqing China Foundry Annual Conference Proceedings*. (2015)
 35. G.C. Manjunath Patel, P. Krishna, M.B. Parappagoudar, Modelling and multi-objective optimisation of squeeze casting process using regression analysis and genetic algorithm. *Aust. J. Mech. Eng.* **14**(3), 182–98 (2015)

Publisher's Note Springer Nature remains neutral with regard to jurisdictional claims in published maps and institutional affiliations.

Springer Nature or its licensor holds exclusive rights to this article under a publishing agreement with the author(s) or other rightsholder(s); author self-archiving of the accepted manuscript version of this article is solely governed by the terms of such publishing agreement and applicable law.